HHS Public Access

Author manuscript

Front Biosci. Author manuscript; available in PMC 2016 January 01.

Published in final edited form as:

Front Biosci. ; 9: 2807–2818.

CONFORMATIONAL SEARCHES ELUCIDATE EFFECTS OF STEREOCHEMISTRY ON STRUCTURES OF DEOXYADENOSINE COVALENTLY BOUND TO TUMORIGENIC METABOLITES OF BENZO[*C*] PHENANTHRENE

Min Wu[1], **S. Frank Yan**[1], **Jian Tan**[1], **Dinshaw J. Patel**[2], **Nicholas E. Geacintov**[1], and **Suse Broyde**[3]

[1] Department of Chemistry, New York University, New York, NY 10003

[2] Cellular Biochemistry and Biophysics Program, Memorial Sloan-Kettering Cancer Center, New York, NY 10021

[3] Department of Biology, New York University, New York, NY 10003

Abstract

Remarkably different conformations can result when DNA binds with stereoisomeric compounds containing differing absolute configurations of substituents about chiral carbon atoms. Furthermore, the biochemical functions of covalent adducts with DNA are strongly affected by the stereochemistry of the ligands. Such stereochemical effects are manifested by DNA covalent adducts derived from metabolites of the non-planar fjord region environmental chemical carcinogen benzo[*c*]phenanthrene. To analyze these phenomena, an extensive conformational investigation for *R* and *S* stereoisomeric adducts to deoxyadenosine, derived from *trans* addition of enantiomeric *anti* diol epoxide metabolites of benzo[*c*]phenanthrene, has been carried out. We have surveyed the potential energy surface of the two adducts by varying systematically at 5° intervals in combination, the three important torsion angles that govern conformational flexibility of the carcinogen bulk with respect to the linked nucleoside. We carried out a grid search by creating 373, 248 structures for each isomer, and evaluated their molecular mechanical energies. This has permitted us to map the potential energy surface of each adduct in these three variables, and to delineate their low energy regions. The maps have a symmetric relationship which stems from the near mirror-image stereochemistry in the *R* and *S* isomers. This produces near mirror-image low energy structures in the nucleoside adducts. The limited sets of stereoisomer-dependent conformational domains delineated are determined by steric effects. Moreover, these features have been experimentally demonstrated to play governing structural roles in such carcinogen-damaged DNA duplexes: opposite orientations in the stereoisomer pairs computed for the nucleosides are observed by high-resolution NMR in the similarly modified DNA double helices, and are likely to play important roles in their interactions with enzymes involved in DNA transactions, and hence their biological activities.

Send correspondence to: Suse Broyde, Ph.D., Department of Biology, New York University, 100 Washington Square East, New York, NY 10003, Tel: 212-998-8231, Fax: 212-995-4015, broyde@nyu.edu or Nicholas E. Geacintov, Ph.D., Department of Chemistry, NY University, 31 Washington Place, NY, NY 10003, Tel: 212-998-8407, Fax: 212-998-8421, ng1@nyu.edu, S. Frank Yan current address: Genomics Institute of the Novartis Research Foundation, San Diego, CA 92121.

Keywords

Conformational search; Potential energy surface; Benzo[c]phenanthrene; Environmental carcinogen; Fjord region polycyclic aromatic hydrocarbon; Stereochemistry and steric effects

2. INTRODUCTION

The biochemical functions of covalent adducts to DNA derived from metabolically activated polycyclic aromatic hydrocarbons (PAHs) are strongly affected by the stereochemistry of the ligands (1-5). Very different conformations can result when DNA binds with stereoisomeric compounds containing differing absolute configurations of substituents about chiral carbon atoms (6). Such stereochemical effects are manifested by DNA adducts derived from metabolites of the environmental chemical carcinogen benzo[*c*]phenanthrene. Benzo[*c*]phenanthrene (B[*c*]Ph) is representative of a class of polycyclic aromatic hydrocarbons (PAHs) containing a crowded fjord region which manifests deviation from planarity of the aromatic ring system (7). Metabolic activation of B[*c*]Ph produces diol epoxides, including a pair of enantiomers (3*R*,4*S*-dihydroxy-1*S*,2*R*-epoxy-1, 2, 3, 4-tetrahydrobenzo[*c*]phenanthrene and the corresponding 3*S*,4*R*,1*R*,2*S* isomer), known as (+)- and (−)-*anti*-B[*c*]PhDE, respectively (Figure 1) (8, 9). DNA can react with these metabolites to form covalently modified duplexes containing these bulky substituents (10). The stereoisomeric 1*R* (+) and 1*S* (−)-*trans*-*anti*-B[*c*]Ph-N^6-dA adducts (Figure 1) are among these. Thermal melting studies revealed that these *R* and *S* adducted DNA duplexes have the same stabilities as the unmodified one (11). In addition, it has been found that they are not repaired by the nucleotide excision repair machinery (2) which removes bulky DNA adducts (12); thus these unrepaired adducts have the chance to encounter the DNA replication machinery. Mutations caused by the unfaithful replication of DNA adducts can contribute to cancer initiation via alteration in function of proto-oncogenes and tumor suppressor genes (13-15). Site specific mutagenesis studies show that the 1*R* (+) and 1*S* (−)-*trans*-*anti*-B[*c*]Ph-N^6-dA adducts have different mutagenic specificities due to the different configurations of the chiral carbon at the linkage point (3).

High resolution NMR solution structures of adenine and guanine-B[*c*]PhDE adducts are available (16-18). These NMR structures reveal intercalation of the B[*c*]Ph moieties into the B-DNA duplex with opposite orientations of insertion with respect to the 5’ direction of the modified strand, in *R* and *S* isomers. The *R* isomer is 5’-directed while the *S* isomer is 3’-directed in adenine adducts (16, 17). In guanine adducts, the *R* isomer is 3’-directed while the *S* isomer is 5’-directed (18). Distorted Watson-Crick base pairing is retained in both cases.

The opposite orientation phenomenon of *R* versus *S* adducts has been extensively documented for the planar, non-hindered bay region PAH benzo[*a*]pyrene (6, 19-22) in both *trans* and *cis* opened guanine and adenine DNA adducts. However, the analogous adducts derived from the fjord region PAH B[*c*]Ph metabolites, which have remarkably different structural features (6) and biochemical functions (2-5, 23) due to the non-planar topology of the aromatic ring system (24), have not been fully investigated (25). As part of an effort to

understand the origins of the structural motifs adopted by both bay and fjord region PAH–DNA adducts, we present results of an extensive computational investigation of the 1*R* (+) and 1*S* (−)-*trans*-*anti*-B[*c*]Ph-N^6-dA adducts (Figure 1) on the nucleoside level. We have surveyed the potential energy surface of these two adducts by varying systematically at 5° intervals in combination, three key sources of conformational flexibility, the torsion angles χ, α' and β' (see Figure 1) of these two adducts. Thus, we created 373, 248 structures for each adduct, and evaluated each of their energies with AMBER 5.0 and the Cornell *et al.* force field (26). This has permitted us to map the potential energy surface of each adduct in these three variables, and to delineate the low energy regions and their relationship in the *R/S* adduct pair.

Our analyses reveal that the conformational preferences manifested on the nucleoside level, governed by stereochemistry, determine the orientations at the duplex DNA level, in these non-planar fjord region adducts. This work thus extends and generalizes a series of computational studies for *R* and *S* adducts of diol epoxide metabolites derived from both the non-planar fjord region benzo[*c*]phenanthrene and the planar bay region benzo[*a*]pyrene. The results show that favored nucleoside conformations govern observed conformational domains at the duplex DNA levels, with steric hindrance effects dominating the potential energy surface in all cases.

3. MATERIALS AND METHODS

3.1. Creating starting conformations

Coordinates of the high resolution NMR solution structure of the 1S (−)-trans-anti-B[c]Ph-N^6-dA adduct in a double stranded DNA 11-mer sequence (17), were employed as the basis for the modified nucleoside structures. The modified nucleoside was excised from the duplex 11-mer of the 1S (−)-trans-anti-B[c]Ph-N^6-dA adduct (17) and the 3' and 5' phosphorus atoms were replaced with hydrogen atoms. For the 1S (−)-trans-anti-B[c]Ph-N^6-dA nucleoside adduct, this served as the starting model. To create a starting model for the 1R (+)-trans-anti-B[c]Ph-N^6-dA, we constructed a mirror-image of the B[c]Ph in the 1S (−)-trans-anti-B[c]Ph-N^6-dA adduct (by inverting the sign of the x coordinates) and then added this moiety to the nucleoside. The conformational details of these structures are given in Table A1, Appendix.

The present study employed fixed conformations for the OH-containing benzylic ring and the fjord region twist. The NMR solution structures in DNA duplexes suggest that these parameters can have some variability (16-18); however, these were not varied in the present comprehensive survey of the potential energy surface for the key torsion angles χ, α', and β' which govern the carcinogen–base orientation, and are the subject of another study (25).

Starting structures for the energy calculations were created with a torsion driver, a program which rotates the torsion angles χ, α' and β' (Figure 1) to chosen values and then computes the coordinates of the resulting structures. The starting structures uniformly surveyed the potential energy surface of the molecule with conformers in which χ, α' and β' sampled their 360° conformation space at 5° intervals, in combination, giving a total of $(360°/5° = 72)^3$ = 373, 248 conformers for each adduct.

3.2. Energy computation

Energies of each of the 373, 248 structures for each adduct were computed with the molecular mechanics program AMBER 5.0 (27), using the Cornell *et al.* force field (26) with the *parm96* parameter set. Since there are no negatively charged phosphates in the nucleoside, Na^+ counterions were not needed. A sigmoidal distance-dependent dielectric function (28) was employed in the Coulombic term of the force field to model the dielectric effects of solvent water.

Parameters added to the AMBER 5.0 force field for the B[*c*]Ph-N^6-dA adducts are the same as those given previously (21), except for the partial charges for the modified nucleosides; these were computed with Gaussian 94 (29) at the 6-31G* basis set level which is compatible with the rest of the Cornell *et al.* force field and *parm96* parameter set; the least squares charge fitting algorithm RESP (30) provided with AMBER 5.0 was then used to fit the charge to each atomic center. Partial charges, atom types and topology information are given in Table A2, Appendix.

Computations were carried out at the Department of Energy's National Energy Research Supercomputer Center (Berkeley, CA), the National Science Foundation National Partnership for Advanced Computational Infrastructure (San Diego, CA) and on our own SGI workstations.

3.3. Statistical weights and thermodynamic quantities

The computed energies were used to construct both three-dimensional energy surfaces as a function of the χ, α', β' torsion angles and two-dimensional energy contour slices through them; slices were made at 5° intervals of χ as a function of α' and β'. The program TECPLOT was used for this purpose. These plots revealed six low-energy wells or domains (Figure 2). This permitted grouping the full data set into six regions, each of which encompassed one of the six low-energy domains:

1. Region 1: χ = 0°–105° and 240°–355°; α' = 270°–355° and 0°–85°; β' for 1*R* (+) adduct = 0°–155°; β' for 1*S* (−) adduct = 200°–355°
2. Region 2: χ = 110°–235°; α' = 270°–355° and 0°–85°; β' for 1*R* (+) adduct = 0°–155°; β' for 1*S* (−) adduct = 200°–355°
3. Region 3: χ =110°–235°; α' = 90°–265°; β' for 1*R* (+) adduct = 0°–155°; β' for 1*S* (−) adduct = 200°–355°
4. Region 4: χ = 0°–105° and 240°–355°; α' = 90°–265°; β' for 1*R* (+) adduct = 0°–155°; β' for 1*S* (−) adduct = 200°–355°
5. Region 5: χ = 0°–105° and 240°–355°; α' = 0°–355°; β' for 1*R* (+) adduct = 160°–355°; β' for 1*S* (−) adduct = 0°–195°
6. Region 6: χ = 110°–235°; α' = 0°–355°; β' for 1*R* (+) adduct = 160°–355°; β' for 1*S* (−) adduct = 0°–195°

With this grouping, we computed fractional statistical weights as well as conformational free energies enthalpies, and entropies as in previous work (19-22).

The fractional statistical weight P_i of each conformer was computed from the relationship:

$$P_i = \frac{e^{-\Delta E_i/RT}}{\sum_{i=1}^{N} e^{-\Delta E_i/RT}}$$

where E_i is the relative energy of a given conformer in kcal/mol with respect to the lowest energy structure, R is the universal gas constant, 1.987×10^{-3} kcal/mol·K, T =300 K, and N is 373, 248, the total number of conformers for each adduct.

Using the above grouping, we computed the combined fractional statistical weight, W_j, for each region (containing one low energy well) by summing the individual statistical weights, P_i, of each point in the region:

$$W_j = \sum_{i=1}^{n_j} P_i$$

where n_j is the number of conformers in each one of the six regions (j = 1, 2, ..., 6).

The conformational free energy of each well, G_j, was then computed from the relationship:

$$G_j = -RT\, ln \sum_{i=1}^{n_j} e^{-\Delta E_i/RT}$$

To obtain the conformational entropy of each well, S_j, we first compute p_i, the fractional statistical weight of each conformer within its own well or region:

$$p_i = \frac{e^{-\Delta E_i/RT}}{\sum_{i=1}^{n_j} e^{-\Delta E_i/RT}}$$

Then,

$$S_j = -R \sum_{i=1}^{n_j} p_i\, ln\, p_i$$

Conformational enthalpies for each well, H_j, are obtained from:

$$G_j = H_j - TS_j$$

Computation of these thermodynamic parameters for each domain treats these as individual chemical species, which appears justifiable on the basis of the apparently high energy barriers between the domains (Figures 2 and 3). The program Insight II from Accelrys, Inc. was employed for computer graphic manipulation and visualization.

4. RESULTS AND DISCUSSION

4.1. Symmetries in potential energy surfaces

The 3-dimensional energy topographies in χ, α' and β' to 6.5 kcal/mol are shown in Figure 2, for the 1*R* (+) and 1*S* (−)-*trans*-*anti*-B[*c*]Ph-N^6-dA adducts. Each adduct has six low energy domains. *Syn* glycosidic torsion angle χ is found in domains I, IV and V, and domains II, III and VI are in the *anti* region. The ranges in the values of χ, α' and β' that characterize the low energy domains are given in Table 1.

Energy contour maps in the α' and β' plane (Figure 3) were created from slices through the approximate centers of the 3-dimensional plots in the *syn* (10°) and *anti* (200°) domains of χ. The 2-dimensional 1*R* (+) and 1*S* (−)-*trans*-*anti* adduct maps are symmetrical: the map for the 1*R* (+) adduct can be essentially transformed into that of the 1*S* (−) adduct by inverting the sign of the torsion angles α' and β', corresponding to an ~180° rotation about a central symmetry axis positioned perpendicular to the map plane at α', β' = 180°, 180°. Thus, a given energy feature in a specific α', β' region of the 1*R* (+) adduct map, has a corresponding feature in the 1*S* (−) adduct map in the −α', −β' region. This torsion angle symmetry is a hallmark of mirror-image pairs of molecules, although the symmetry is not exact in our nucleoside adduct pair.

The α', β' energy contour maps at 5° intervals of χ for each adduct reveal the same symmetries as in Figure 3. Table A3, Appendix, gives the number of conformers in 1 kcal/mol shells and Table 2 gives computed thermodynamic parameters and statistical weights. Differences in population between the structures of the 1*R* (+) and 1*S* (−) adduct stem from the symmetry breaking effect of the sugar residues and C4'-C5' atoms. We note that domain IV (discussed below) is the most preferred domain, and that favorable conformational entropy plays the key part in stabilizing it.

4.2. Near mirror-image symmetries in low energy conformations

Color views of representative structures of each of the six low energy domains of the 1*R* (+) and 1*S* (−)-*trans*-*anti* adducts are shown in Figure 4. The 1*R* (+) adduct structure is nearly a mirror-image of the 1*S* (−) one in each domain, with the mirror-image symmetry broken by the sugars, whose O4' atoms point in the same rather than the opposite directions in each pair.

4.3. Structural domain preferences

Syn and Anti Conformations—Domains I (*syn*) and II (*anti*) are essentially the same except for the difference in glycosidic torsion angles. The stabilization of domain I relative to domain II probably stems from the fact that the sugar residue has favorable interactions with both aromatic rings of the adenine in the *syn* conformation; when the adenine residue is in the *anti* orientation, the sugar contacts only its 5-membered ring. This characteristic is intrinsic to the deoxyadenosine moiety and is not significantly influenced by the B[*c*]Ph residue. *Syn* domains IV and V are favored over *anti* domains III and VI, respectively, for the same reason. The *syn* domain preference in nucleosides is overcome in DNA duplexes

through maintenance of Watson-Crick base pairing, which requires the *anti* domain in B-DNA, as discussed below.

α' and β' Regions—Table 1 reveals that α' is centered at 0° or 180° in each of the low energy domains, and Table 2 shows that the α'=180° region is favored more. The preference for these two α' regions stems from the maximal overlap of the adenine aromatic ring π orbitals with the N^6 lone pair p orbital when α' = ~0° or ~180°.

With these α' values, the preferred β' are the 90° region for the 1*R* (+) isomer and the 270° (− 90°) region for the 1*S* (−) isomer; other combinations of α' and β' produced crowded structures. In normal B-DNA duplexes, the α' = ~180° region is required to form the Watson-Crick hydrogen bond that involves the free hydrogen atom on N^6-dA (6).

4.4. Steric hindrance produces opposite orientations in *R* and *S* isomers

Energy contour maps in the α', β' plane which considered only the van der Waals component of the total energy helped to elucidate the origin of the opposite orientations (Figure 5). For each adduct, these maps contain the same overall regions below 25 kcal/mol, with the same symmetry effects as those employing the full energy potential (Figure 3). The energy boundaries above 25 kcal/mol are determined by repulsive steric components of the Lennard-Jones potential employed to compute van der Waals energies (31), and hence steric repulsions are predominantly responsible for the different energy landscapes in the 1*R* (+) and 1*S* (−)-*trans* adducts and for the symmetries between them. The energy regions below 25 kcal/mol contain differing details in the total energy maps (Figure 3) than in the van der Waals component maps (Figure 5), due to modulating effects of electrostatic, torsional and other terms in the total energy.

To further examine the nature of the steric repulsions, we rotated each structure shown in Figure 4 into that preferred by its stereoisomer, a 180° rotation around β' in each case. For domains I and II of both 1*R* (+) and 1*S* (−) adducts, after rotation, the N1 of the purine is in a crowded region with the C4A, C4B and H3 of the B[*c*]Ph moiety; for domains III and IV, the rotated structures show crowding between N7 of the adenine and C4A, C4B and H3 of the B[*c*]Ph; the rotated structures of domains V and VI, however, show no crowding. After rotation, domains V and VI are close to allowed domains I and II, respectively. The crowding between atoms on the adenine and the benzylic ring of the B[*c*]Ph residues caused by rotation of β' from the region preferred by one stereoisomer into the region preferred by the other has been termed "primary" steric hindrance (6).

4.5. Nucleoside conformations govern solution structures of DNA duplexes

The footnote to Table 1 summarizes the χ, α', β' values adopted by the 1*R* (+) and 1*S* (−)-*trans*-*anti*-B[*c*]Ph-N^6-dA adducts (16, 17) in double stranded DNA, determined from the analysis of high resolution NMR solution data. Both of the B[*c*]Ph NMR solution structures adopt α', β' combinations in the vicinity of domain IV, which is most favored for each adduct on the nucleoside level (Table 2). In the observed domain IV, the B[*c*]Ph moiety is placed on the 3'-side of the modified adenine in the 1*S* (−)-*trans*-*anti* adduct, and on the 5'-side in the 1*R* (+)-*trans*-*anti*-isomeric adduct in nucleosides and duplexes. However, in the

duplexes distorted Watson-Crick base pairing is maintained. This is permitted by the 180° region adopted by torsion angle α' (Figures 4 and 6), but also requires the *anti* domain for the glycosidic torsion angle χ, found on the nucleoside level in Domain III. The torsion angle β' adopts values of ~ −90° for the 1*S* (−) and ~ +90° for the 1*R* (+)-*trans*-*anti* isomer (Table 1). Thus, the α', β' combination, computed in nucleosides and observed in duplexes, gives rise to the opposite orientations of the B[*c*]Ph, relative to the modified deoxyadenosyl residues.

These results are consistent with our previous studies on *R* and *S* benzo[*c*]phenanthrene diol epoxide guanine adducts (25), and on a number of *R* and *S* nucleoside adducts of diol epoxide metabolites derived from the planar bay region PAH, benzo[*a*]pyrene (19-22). In all cases symmetric potential energy surfaces are manifested in nucleosides and opposite orientations are observed in NMR solution structures of DNA duplexes (18, 32-35). Thus, our findings regarding opposite orientations of *S* and *R* isomers appear to be general, encompassing both planar bay and non-planar fjord region PAHs. The particular type of conformational theme adopted by the aromatic moiety in DNA duplexes, namely (1) at the helix exterior in a groove; (2) inserted into the helix with displacement of the covalently modified base to the helix exterior; or (3) intercalation with maintenance of Watson–Crick base pairing, is governed by a subtle interplay of hydrogen bonding, hydrophobic and steric forces involving both the aromatic ring of the carcinogen and the DNA (6). These are determined by the specific stereochemistry and adduction site of the differing isomers. Modulating conformational effects, stemming from flexibility in benzylic ring conformation and non-planarity in the aromatic ring system, observed in the NMR solution structures of these sterically hindered fjord region adducts (16-18) are considered in another investigation (25). However, opposite orientations are adopted by *R* and *S* stereoisomers irrespective of the specific conformational theme. It is quite remarkable that the opposite orientations in all polycyclic aromatic *R* and *S* adducted duplexes observed so far can be fully explained by the nucleoside conformations. These structural distinctions may play a role in producing differential mutagenic specificities observed in *R* and *S* isomeric adducts (3, 4, 36)

5. BIOLOGICAL IMPLICATIONS

Our comprehensive survey of the potential energy surface for a stereoisomeric pair of small molecules, namely carcinogen-linked nucleosides, defined the energetic and structural features which govern the orientation of the carcinogen with respect to its covalently bound base. The computations delineated limited sets of allowed conformational domains that are stereoisomer-dependent and determined by steric effects. These features have been experimentally demonstrated to play governing structural roles in such carcinogen-damaged DNA duplexes: opposite orientations in the stereoisomer pairs computed for the nucleosides are observed by high-resolution NMR in the similarly modified DNA double helices. It is plausible that the favored conformational domains would occur within enzymes that process these lesions. Observed differences in biological activities such as mutagenicity in the stereoisomer pair likely result from differential treatment by polymerases, which stem from the opposite orientations. Finally, this study underscores the power of the conformational searches to define conformations of small, biologically important molecules of limited flexibility, reveals their applicability to relevant macromolecules, and points to functional

implications of the structural findings. Analogous approaches in defining conformational features, the role of stereochemistry, and their relation to biological activity in small ligands that may interact with proteins can be useful techniques in computer aided drug discovery.

ACKNOWLEDGEMENTS

This research is supported by NIH grant CA-28038 to S.B., NIH grant CA-46533 to D.J.P., and NIH grant CA-20851 to N.E.G.

8. APPENDIX

Table A1

Conformational Features of Modified Nucleosides

Dihedral Angle	1*R* (+)-*trans*-*anti*-B[*c*]Ph-N^6-A (deg)	1*S* (–)-*trans*-*anti*-B[*c*]Ph-N^6-A (deg)
C1-C2-C3-C4	54.30	−54.30
C2-C3-C4-C4A	−48.71	48.71
C3-C4-C4A-C1A	27.41	−27.41
C4-C4A-C1A-C1	−9.14	9.14
C4A-C1A-C1-C2	14.28	−14.28
C1A-C1-C2-C3	−38.00	38.00
C1-C2-O2-HO2	51.30	51.30
C2-C3-O3-HO3	−71.79	71.79
C3-C4-O4-HO4	−62.15	62.15
C4B-C6B-C8B-C12	15.78	−15.78
C1-C4B-C6B-C8B	9.15	−9.15
O4N-C1N-C2N-C3N	37.16	37.16
C1N-C2N-C3N-C4N	−36.55	−36.55
C2N-C3N-C4N-O4N	23.63	23.63
C3N-C4N-O4N-C1N	−0.44	−0.44
C4N-O4N-C1N-C2N	−23.22	−23.22
O4N-C4N-C5N-O5N	−56.54	−56.54
C4N-C5N-O5N-H5N	2.40	2.40
C2N-C3N-O3N-H3N	−39.79	−39.79
C3N-C4NC5N-O5N	62.26	62.26

Table A2

Partial Charges, Topology, and Atom Type Assignments

				Charges	
Atom		Type	Topology	1R(+)-B[c]Ph	1S(–)-B[c]Ph
dA:	HO5	HO	M	0.369402	0.384554
	O5′	OH	M	−0.597676	−0.640506
	C5′	CT	M	0.063023	0.215272

				Charges	
Atom		Type	Topology	1R(+)-B[c]Ph	1S(–)-B[c]Ph
	H5′1	H1	E	0.077803	0.032584
	H5′2	H1	E	0.121727	0.075972
	C4′	CT	M	0.032341	0.003844
	H4′	H1	E	0.115023	0.093768
	O1′	OS	S	−0.356514	−0.350765
	C1′	CT	B	0.054737	−0.002370
	H1′	H2	E	0.127963	0.199964
	N9	N*	S	0.039077	−0.029234
	C8P	CK	B	−0.016961	0.051096
	H8P	H5	E	0.173580	0.192984
	N7	NB	S	−0.427606	−0.485960
	C5P	CB	S	0.024748	0.071670
	C4P	CB	S	0.375799	0.411124
	N3	NC	S	−0.688109	−0.737523
	C2P	CQ	B	0.591722	0.627065
	H2P	H5	E	0.046343	0.040777
	N1	NC	S	−0.644863	−0.654923
	C6P	CA	S	0.483293	0.463303
	N6	N2	B	−0.562482	−0.546219
	HN6	H	E	0.333586	0.329206
	C3′	CT	M	0.205377	0.337776
	H3′	H1	E	0.126271	0.093759
	C2′	CT	B	−0.130653	−0.267874
	H2′1	HC	E	0.083002	0.118957
	H2′2	HC	E	0.067844	0.075082
	O3′	OH	M	−0.651333	−0.673750
	HO3	HO	M	0.408315	0.413234
B[c]Ph:	C1Z	CT	B	−0.012501	0.009626
	H1Z	H1	E	0.148079	0.128628
	C2Z	CT	3	0.009910	0.067960
	H2Z	H1	E	0.156274	0.147212
	O2Z	OH	S	−0.600130	−0.610844
	HO2Z	HO	E	0.373496	0.372272
	C3Z	CT	3	0.201143	0.200388
	H3Z	H1	E	0.111411	0.094092
	O3Z	OH	S	−0.657781	−0.659476
	HO3Z	HO	E	0.426531	0.419514
	C4Z	CT	3	0.156935	0.226752

				Charges	
Atom		Type	Topology	1R(+)-B[c]Ph	1S(–)-B[c]Ph
	H4Z	H1	E	0.037687	0.015203
	O4Z	OH	S	−0.631642	−0.644431
	HO4Z	HO	E	0.411246	0.411158
	C4A	CA	S	0.020305	0.002818
	C5Z	CA	B	−0.126848	−0.150585
	H5Z	HA	E	0.145944	0.149816
	C6Z	CA	B	−0.234776	−0.201667
	H6Z	HA	E	0.161741	0.155844
	C6A	CA	S	0.064061	0.065413
	C7Z	CA	B	−0.125625	−0.164495
	H7Z	HA	E	0.130481	0.137207
	C8Z	CA	B	−0.267977	−0.215210
	H8Z	HA	E	0.155668	0.144279
	C8A	CA	S	0.179590	0.148056
	C9Z	CA	B	−0.209005	−0.214245
	H9Z	HA	E	0.147059	0.152141
	C10	CA	B	−0.136028	−0.150137
	H10	HA	E	0.136226	0.138240
	C11	CA	B	−0.110064	−0.060934
	H11	HA	E	0.138868	0.108273
	C12	CA	B	−0.236757	−0.301061
	H12	HA	E	0.167586	0.194036
	C8B	CA	S	0.065726	0.089404
	C6B	CA	S	−0.011029	0.010791
	C4B	CA	E	−0.030583	−0.058906

Table A3

Number of Conformations in 1 kcal/mol Shells in 1*R* (+) and 1*S* (–)-*trans*-*anti*-B[*c*]Ph-N^6-dA Adducts, to 5 kcal/mol

	0-1 kcal/mol		1-2 kcal/mol		2-3 kcal/mol		3-4 kcal/mol		4-5 kcal/mol		Total	
Domain	**(+)**	**(–)**	**(+)**	**(–)**	**(+)**	**(–)**	**(+)**	**(–)**	**(+)**	**(–)**	**(+)**	**(–)**
I	0	0	81	127	430	462	629	621	780	766	1920	1976
II	0	0	0	0	0	0	0	0	3	110	3	110
III	0	0	0	0	0	1	93	297	429	485	522	783
IV	211	188	395	395	530	520	555	560	785	784	2476	2447
V	0	0	0	0	113	93	306	312	489	455	908	860
VI	0	0	0	0	0	0	0	0	0	0	0	0
Total	211	188	476	522	1073	1076	1583	1790	2486	2600	5829	6176

REFERENCES

1. Chary P, Lloyd RS. *In vitro* replication by prokaryotic and eukaryotic polymerases on DNA templates containing site-specific and stereospecific benzo[*a*]pyrene-7, 8-dihydrodiol-9, 10-epoxide adducts. Nucleic Acids Res. 1995; 23:1398–1405. [PubMed: 7753632]
2. Buterin T, Hess MT, Luneva N, Geacintov NE, Amin S, Kroth H, Seidel A, Naegeli H. Unrepaired fjord region polycyclic aromatic hydrocarbon-DNA adducts in *ras* codon 61 mutational hot spots. Cancer Res. 2000; 60:1849–1856. [PubMed: 10766171]
3. Ponten I, Sayer JM, Pilcher AS, Yagi H, Kumar S, Jerina DM, Dipple A. Factors determining mutagenic potential for individual cis and trans opened benzo[*c*]phenanthrene diol epoxide-deoxyadenosine adducts. Biochemistry. 2000; 39:4136–4144. [PubMed: 10747805]
4. Ramos LA, Ponten I, Dipple A, Kumar S, Yagi H, Sayer JM, Kroth H, Kalena G, Jerina DM. Site-specific mutagenesis in *Escherichia coli* by *N*2-deoxyguanosine adducts derived from the highly carcinogenic fjord-region benzo[*c*]phenanthrene 3, 4-diol 1, 2-epoxides. Chem Res Toxicol. 2002; 15:1619–1626. [PubMed: 12482245]
5. Rechkoblit O, Zhang Y, Guo D, Wang Z, Amin S, Krzeminsky J, Louneva N, Geacintov NE. Translesion synthesis past bulky benzo[*a*]pyrene diol epoxide N2-dG and N6-dA lesions catalyzed by DNA bypass polymerases. J Biol Chem. 2002; 277:30488–30494. [PubMed: 12063247]
6. Geacintov NE, Cosman M, Hingerty BE, Amin S, Broyde S, Patel DJ. NMR solution strucutures of stereoisomeric covalent polycyclic aromatic carcinogen-DNA adducts: principles, patterns, and diversity. Chem Res Toxicol. 1997; 10:111–146. [PubMed: 9049424]
7. Hirshfeld FL. The structure of overcrowded aromatic compounds. Part VII. Out-of-plane deformation in benzo[*c*] phenanthrene and 1, 12-dimethyl-benzo[*c*]phenanthrene. J Chem Soc. 1963:2126–2135.
8. Levin W, Wood AW, Chang RL, Ittah Y, Croisy-Delcey M, Yagi H, Jerina DM, Conney AH. Exceptionally high tumor-initiating activity of benzo[*c*]phenanthrene bay-region diol-epoxides on mouse skin. Cancer Res. 1980; 40:3910–3914. [PubMed: 7471042]
9. Thakker DR, Levin W, Yagi H, Yeh HJ, Ryan DE, Thomas PE, Conney AH, Jerina DM. Stereoselective metabolism of the (+)-(*S*,*S*)- and (−)-(*R*,*R*)-enantiomers of trans-3, 4-dihydroxy-3, 4-dihydrobenzo[*c*]-phenanthrene by rat and mouse liver microsomes and by a purified and reconstituted cytochrome P-450 system. J Biol Chem. 1986; 261:5404–5413. [PubMed: 3957930]
10. Agarwal SK, Sayer JM, Yeh HJC, Pannell LK, Hilton BD, Pigott MA. Chemical characterization of DNA adducts derived from the configurationally isomeric benzo[*c*]phenanthrene-3, 4-diol-1, 2-epoxides. J Am Chem Soc. 1987:2497–2504.
11. Laryea A, Cosman M, Lin JM, Liu T, Agarwal R, Smirnov S, Amin S, Harvey RG, Dipple A, Geacintov NE. Direct synthesis and characterization of site-specific adenosyl adducts derived from the binding of a 3, 4-dihydroxy-1, 2-epoxybenzo[*c*]phenanthrene stereoisomer to an 11-mer oligodeoxyribonucleotide. Chem Res Toxicol. 1995; 8:444–454. [PubMed: 7578932]
12. Wood RD. DNA damage recognition during nucleotide excision repair in mammalian cells. Biochimie. 1999; 81:39–44. [PubMed: 10214908]
13. Weinberg RA. How cancer arises. Sci Am. 1996; 275:62–70. [PubMed: 8701295]
14. Garner RC. The role of DNA adducts in chemical carcinogenesis. Mutat Res. 1998; 402:67–75. [PubMed: 9675247]
15. Gibbs WW. Untangling the roots of cancer. Sci Am. 2003; 289:56–65. [PubMed: 12840947]
16. Cosman M, Fiala R, Hingerty BE, Laryea A, Lee H, Harvey RG, Amin S, Geacintov NE, Broyde S, Patel D. Solution conformation of the (+)-*trans*-*anti*-[BPh]dA adduct opposite dT in a DNA duplex: intercalation of the covalently attached benzo[*c*]phenanthrene to the 5′-side of the adduct site without disruption of the modified base pair. Biochemistry. 1993; 32:12488–12497. [PubMed: 8241140]
17. Cosman M, Laryea A, Fiala R, Hingerty BE, Amin S, Geacintov NE, Broyde S, Patel DJ. Solution conformation of the (−)-*trans*-*anti*-benzo[*c*]phenanthrene-dA ([BPh]dA) adduct opposite dT in a DNA duplex: intercalation of the covalently attached benzo[*c*]phenanthrenyl ring to the 3′-side of the adduct site and comparison with the (+)-*trans*-*anti*-[BPh]dA opposite dT stereoisomer. Biochemistry. 1995; 34:1295–1307. [PubMed: 7827077]

18. Lin C, Huang X, Kolbanovskii A, Hingerty BE, Amin S, Broyde S, Geacintov NE, Patel DJ. Molecular topology of polycyclic aromatic carcinogens determines DNA adduct conformation: a link to tumorigenic activity. J Mol Biol. 2001; 306:1059–1080. [PubMed: 11237618]
19. Xie XM, Geacintov NE, Broyde S. Stereochemical origin of opposite orientations in DNA adducts derived from enantiomeric anti-benzo[*a*]pyrene diol epoxides with different tumorigenic potentials. Biochemistry. 1999; 38:2956–2968. [PubMed: 10074348]
20. Xie XM, Geacintov NE, Broyde S. Origins of conformation differences between cis and trans DNA adducts derived from enantiomeric *anti*-benzo[*a*]pyrene diol epoxides. Chem Res Toxicol. 1999; 12:597–609. [PubMed: 10409399]
21. Tan J, Geacintov NE, Broyde S. Principles governing conformations in stereoisomeric adducts of bay region benzo[*a*]pyrene diol epoxides to adenine in DNA: steric and hydrophobic effects are dominant. J Am Chem Soc. 2000; 122:3021–3032.
22. Tan J, Geacintov NE, Broyde S. Conformational determinants structures in stereoisomeric *cis*-opened *anti*-benzo[*a*]pyrene diol epoxide adducts to adenine in DNA. Chem Res Toxicol. 2000; 13:811–822. [PubMed: 10995253]
23. Frank EG, Sayer JM, Kroth H, Ohashi E, Ohmori H, Jerina DM, Woodgate R. Translesion replication of benzo[*a*]pyrene and benzo[*c*]phenanthrene diol epoxide adducts of deoxyadenosine and deoxyguanosine by human DNA polymerase ι. Nucleic Acids Res. 2002; 30:5284–5292. [PubMed: 12466554]
24. Wu M, Yan S, Patel DJ, Geacintov NE, Broyde S. Relating repair susceptibility of carcinogen-damaged DNA with structural distortion and thermodynamic stability. Nucleic Acids Res. 2002; 30:3422–3432. [PubMed: 12140327]
25. Wu M, Yan S, Patel DJ, Geacintov NE, Broyde S. Cyclohexene ring and fjord region twist inversion in stereoisomeric DNA adducts of enantiomeric benzo[*c*]phenanthrene diol epoxides. Chem Res Toxicol. 2001; 14:1629–1642. [PubMed: 11743746]
26. Cornell WD, Cieplak P, Bayly CI, Gould IR, Merz KM, Ferguson DM, Spellmeyer DC, Fox T, Caldwell JW, Kollman PA. A second generation force field for the simulation of proteins and nucleic acids. J Am Chem Soc. 1995; 117:5179–5197.
27. Case, D.; Pearlman, D.; Caldwell, J.; Cheatham, T.; Ross, W.; Simmerling, C.; Darden, T.; Merz, K.; Stanton, R.; Cheng, A.; Vincent, J.; Crowley, M.; Ferguson, D.; Radner, R.; Seibel, G.; Singh, UC.; Weiner, P.; Kollman, P. AMBER 5.0. University of California; San Francisco, CA: 1997.
28. Hingerty BE, Ritchie RH, Ferrell TL, Turner JE. Dielectric effects in biopolymers: the theory of inonic saturation revisited. Biopolymers. 1985; 24:427–439.
29. Frisch, MJ.; Trucks, GW.; Schlegel, HB.; Gill, P.; Johnsone, BG.; Robb, MA.; Cheeseman, JR.; Keith, TA.; Petersson, GA.; Montgomery, JA.; Raghavachari, K.; Al-Laham, MA.; Zakrzewski, VG.; Ortiz, JV.; Foresman, JB.; Cioslowski, J.; Stefanov, BB.; Nanayakkara, A.; Challacombe, M.; Peng, CY.; Ayala, PY.; Chen, W.; Wong, MW.; Andres, JL.; Reploge, ES.; Gomperts, R.; Martin, RL.; Fox, DJ.; Binkley, JS.; Defrees, DJ.; Baker, J.; Stewart, JP.; Head-Gordon, M.; Gonzalez, C.; Pople, JA. Gaussian 94 (Revision A.1). Pittsburgh PA: 1995.
30. Bayly CI, Cieplak P, Cornell WD, Kollman PA. A well-behaved electrostatic potential based method using charge restraints for deriving atomic charges: the RESP model. J Phys Chem. 1993; 97:10269–10280.
31. Atkins, PW. Physical Chemistry. 4th ed.. W. H. Freeman Co.; New York: 1990.
32. Cosman M, de los Santos C, Fiala R, Hingerty BE, Singh SB, Ibanez V, Margulis LA, Live D, Geacintov NE, Broyde S. Solution conformation of the major adduct between the carcinogen (+)-*anti*-benzo[*a*]pyrene diol epoxide and DNA. Proc Natl Acad Sci USA. 1992; 89:1914–1918. [PubMed: 1311854]
33. Cosman M, de los Santos C, Fiala R, Hingerty BE, Ibanez V, Luna E, Harvey R, Geacintov NE, Broyde S, Patel DJ. Solution conformation of the (+)-*cis*-*anti*-[BP]dG adduct in a DNA duplex: intercalation of the covalently attached benzo[*a*]pyrenyl ring into the helix and displacement of the modified deoxyguanosine. Biochemistry. 1993; 32:4145–4155. [PubMed: 8476845]
34. Cosman M, Hingerty BE, Luneva N, Amin S, Geacintov NE, Broyde S, Patel DJ. Solution conformation of the (−)-*cis*-*anti*-benzo[*a*]pyrenyl-dG adduct opposite dC in a DNA duplex: intercalation of the covalently attached BP ring into the helix with base displacement of the

modified deoxyguanosine into the major groove. Biochemistry. 1996; 35:9850–9863. [PubMed: 8703959]

35. de los Santos C, Cosman M, Hingerty BE, Ibanez V, Margulis LA, Geacintov NE, Broyde S, Patel DJ. Influence of benzo[*a*]pyrene diol epoxide chirality on solution conformations of DNA covalent adducts: the (−)-*trans*-*anti*-[BP]G.C adduct structure and comparison with the (+)-*trans*-*anti*-[BP]G.C enantiomer. Biochemistry. 1992; 31:5245–5252. [PubMed: 1606148]
36. Ponten I, Kroth H, Sayer JM, Dipple A, Jerina DM. Differences between the mutational consequences of replication of *cis*- and *trans*-opened benzo[*a*]pyrene 7, 8-diol 9, 10-epoxidedeoxyguanosine adducts in M13mp7L2 constructs. Chem Res Toxicol. 2001; 14:720–726. [PubMed: 11409943]

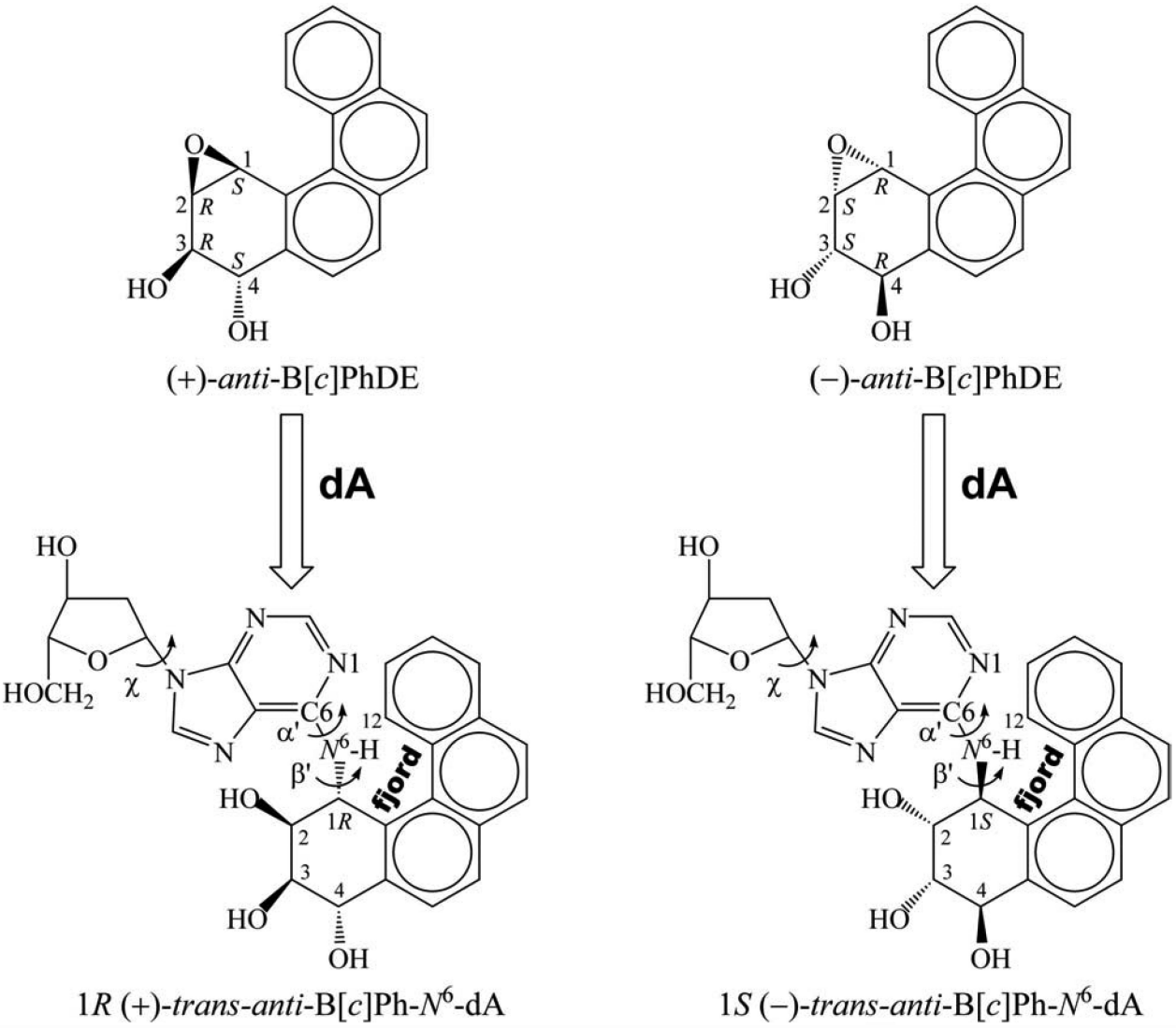

Figure 1.

Structures of (+) and (−)-*anti*-B[*c*]PhDE and of 1*R* (+) and 1*S* (−)-*trans*-*anti*-B[*c*]Ph-N^6-dA nucleoside adducts. Torsion angles χ, α', β' are defined as follows: χ, O4'-C1'-N9-C4; α', N1-C6-N^6-C1 (B[*c*]Ph); β', C6- N^6-C1(B[*c*]Ph)-C2(B[*c*]Ph). The fjord region encompasses the C1-C12 area.

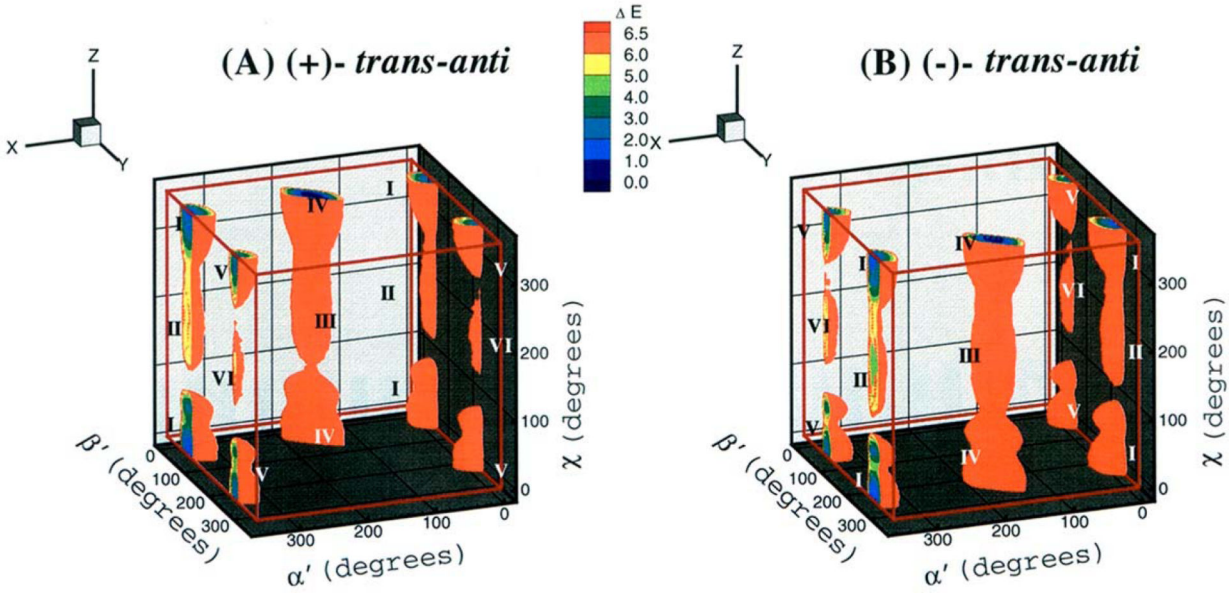

Figure 2.

Three-dimensional χ, α' and β' energy topographies to 6.5 kcal/mol. I-VI denote the 6 low energy domains. (A), 1*R*(+)-*trans-anti*-B[*c*]Ph-N^6-dA adduct; (B), 1*S* (−)-*trans-anti*-B[*c*]Ph-N^6-dA adduct.

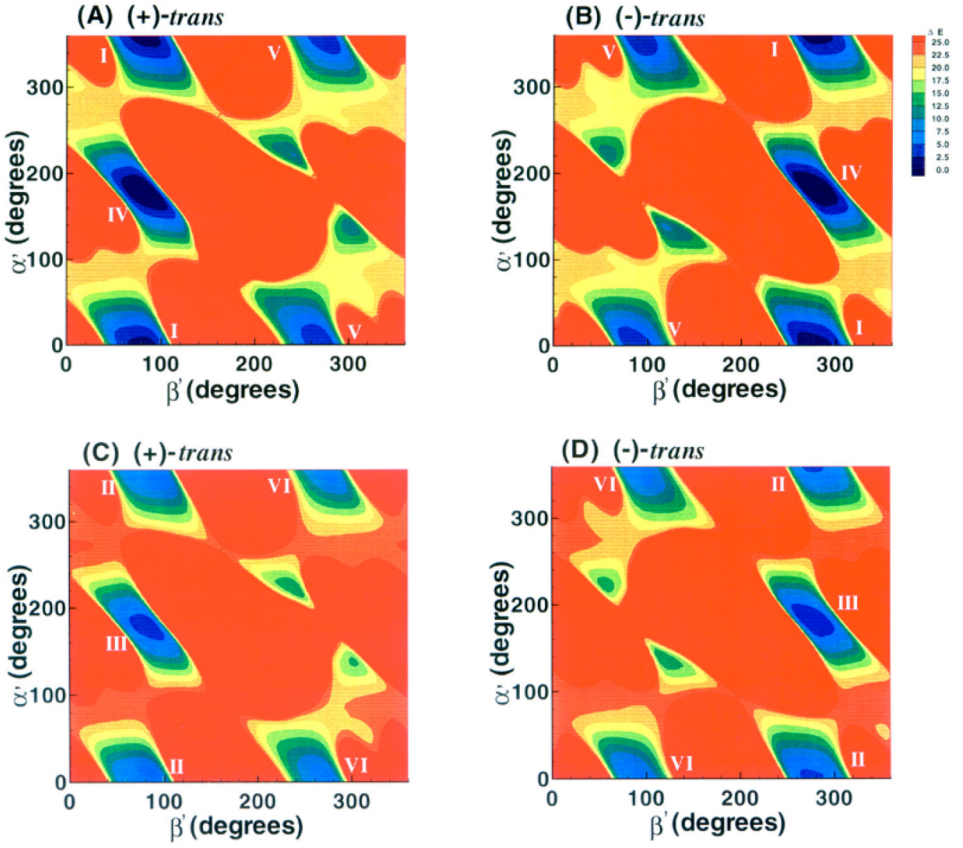

Figure 3.

α', β' energy contour maps to 25 kcal/mol. (A), 1*R* (+)-*trans*-*anti*-B[*c*]Ph-N^6-dA adduct, χ = 10° (*syn*); (B), 1*S* (−)-*trans*-*anti*-B[*c*]Ph-N^6-dA adduct, χ = 10° (*syn*); (C), 1*R* (+)-*trans*-*anti*-B[*c*]Ph-N^6-dA adduct, χ = 200° (*anti*); (D), 1*S* (−)-*trans*-*anti*-B[*c*]Ph-N^6-dA adduct, χ = 200° (*anti*).

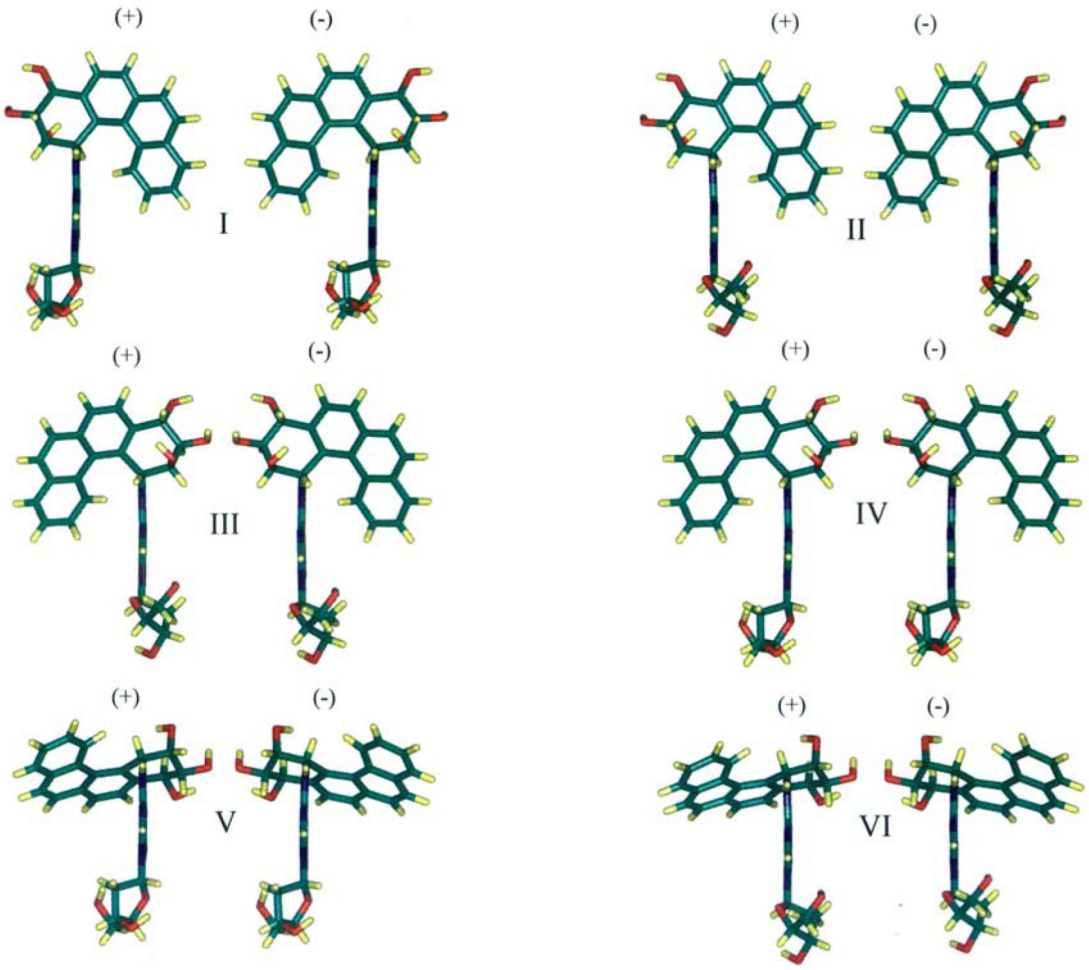

Figure 4.

Color views of representative structures for 1*R* (+) and 1*S* (−)-*trans-anti*-B[*c*]Ph-N^6-dA adducts. In each pair the left structure is the 1*R* (+)-*trans-anti*-B[*c*]Ph-N^6-dA adduct and the right is the 1*S* (−) adduct. χ, α', and β' values and energies, Δ*E*, relative to the global minimum are the following. Domain I: 1*R* (+) adduct 10°, 0°, 90°; 1*S* (−) adduct 10°, 0°, 270°; Δ*E* +1.85, −1.36 kcal/mol. Domain II: 1*R* (+) adduct 200°, 0°, 90°; 1*S* (−) adduct 200°, 0°, 270°; Δ*E* +5.14, −4.73 kcal/mol. Domain III: 1*R* (+) adduct 200°, 180°, 90°; 1*S* (−) adduct: 200°, 180°, 270°; Δ*E* +3.87, −3.20 kcal/mol. Domain IV: 1*R* (+) adduct 10°, 180°, 90°; 1*S* (−) adduct 10°, 180°, 270°; Δ*E* +0.55, −0.22 kcal/mol. Domain V: 1*R* (+) adduct 10°, 0°, 270°; 1*S* (−) adduct 10°, 0°, 90°; Δ*E* +2.55, −2.28 kcal/mol. Domain VI: 1*R* (+) adduct 200°, 0°, 270°; 1*S* (−) adduct 200°, 0°, 90°; Δ*E* +6.01, −5.47 kcal/mol. The view is edge-on along the adenine with C8H directed toward the viewer.

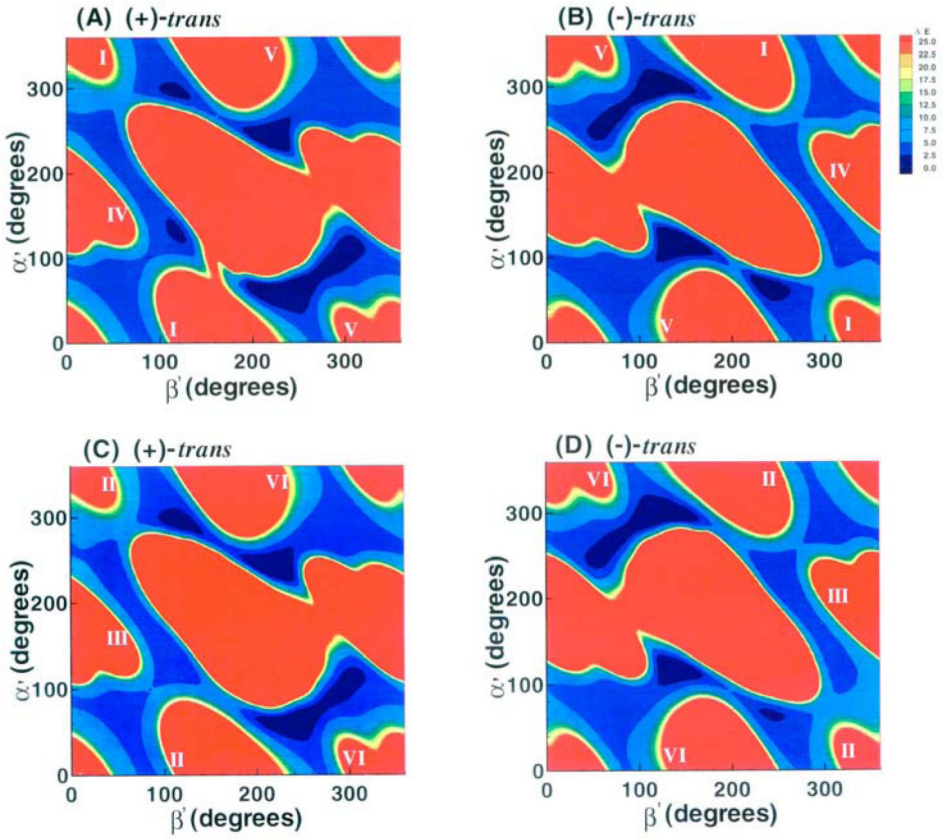

Figure 5.

α', β' van der Waals energy component maps to 25 kcal/mol. (A), 1*R* (+)-trans-anti-B[*c*]Ph-N^6-dA adduct, χ = 10° (*syn*); (B), 1*S*(−)-*trans*-*anti*-B[*c*]Ph-N^6-dA adduct, χ = 10° (*syn*); (C), 1*R* (+)-*trans*-*anti*-B[*c*]Ph-N^6-dA adduct, χ = 200° (*anti*); (D), 1*S*(−)-*trans*-*anti*-B[*c*]Ph-N^6-dA adduct, χ = 200° (*anti*).

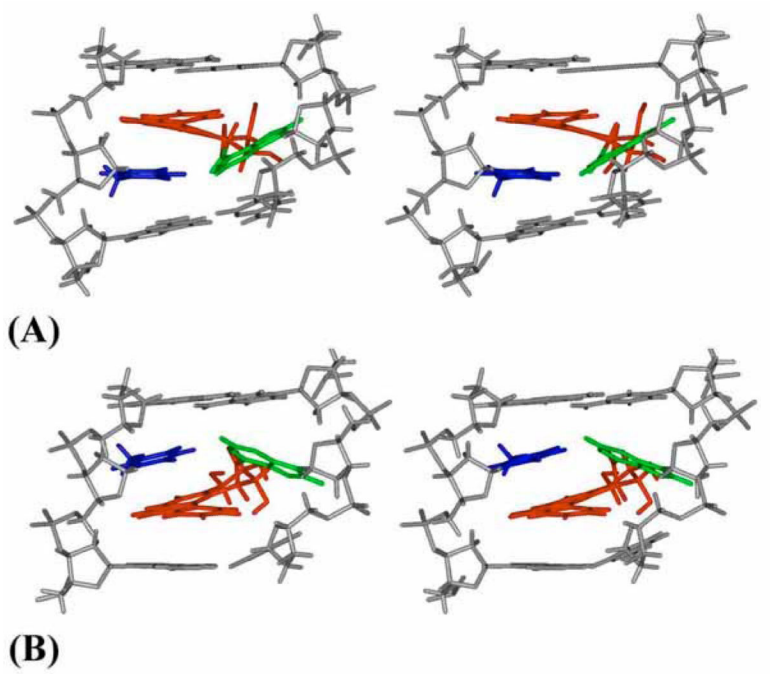

Figure 6.

Stereo views of central modified duplex 5-mer NMR solution structures. The (A) 1*R* (+)-*trans*-*anti*-B[*c*]Ph-N^6-dA (16) and (B) 1*S* (−)-*trans*-*anti*-B[*c*]Ph-N^6-dA (17) adducts. B[*c*]Ph is red, modified adenine is green, and the partner thymine is blue. Backbone, sugar, and other nucleotide atoms are in gray.

Table 1

Domains of Low-Energy Wells in 1*R* (+) and 1*S* (–)-*trans*-*anti*-B[*c*]Ph-N^6-dA Adducts [1]

	χ domain	α' domain	β' domain(deg)	
			(+)	(–)
domain	**(deg)**	**(deg)**	**Adduct**	**Adduct**
I	10 + 100/– 130	0 + 40/– 45	90 + 35/–55	270 + 55/– 35
II	200 + 40/– 90	0 ± 30	90 + 25/– 45	270 + 45/– 25
III	200 + 40/– 90	180 + 40/– 35	90 + 25/– 50	270 + 50/– 25
IV	10 + 100/– 130	180 + 45/– 50	90 + 40/– 60	270 + 60/– 40
V	10 + 100/– 130	0 + 45/– 40	270 + 35/– 45	90 + 45/– 35
VI	200 + 40/– 90	0 + 35/– 30	270 ± 25	90 ± 25

[1]Domains of the 10 kcal/mol surface were approximated to ±5°; χ, α', β' orientations in NMR solution structures of 1*R* (+) and 1*S* (–)-*trans*-*anti*-B[*c*]Ph-N^6-dA adducts: 1*R* (+) adduct 232°, 154°, and 104°, respectively (16); 1*S* (–) adduct 294°, 229°, and 249°, respectively (17).

Table 2

Computed Statistical Weights and Thermodynamics Parameters for Low-Energy Domains in 1*R* (+) and 1*S* (–)-*trans*-*anti*-B[*c*]Ph-N^6-dA Adducts [a]

	W%		G		H		TS	
			(kcal/mol)		(kcal/mol)		(kcal/mol)	
Domain	**(+)**	**(–)**	**(+)**	**(–)**	**(+)**	**(–)**	**(+)**	**(–)**
I	9.440	12.593	–1.537	–1.687	2.464	2.287	4.001	3.974
II	0.044	0.082	1.666	1.313	5.756	5.391	4.090	4.078
III	0.338	0.812	0.448	–0.052	4.345	3.856	3.896	3.909
IV	88.430	84.785	–2.871	–2.824	0.955	0.997	3.826	3.821
V	1.741	1.714	–0.529	–0.498	3.240	3.249	3.769	3.747
VI	0.007	0.014	2.760	2.376	6.613	6.226	3.853	3.849

[a]Statistical weights, *W*, are given in percents of the population. *G*, *H*, and *S* are conformational free energy, enthalpy, and entropy, respectively. *T* = 300 K